
DISTILLING LLM REASONING INTO GRAPH OF CONCEPT PREDICTORS

A PREPRINT

Ziyang Yu

Department of Computer Science
Emory University
Atlanta, USA
ziyang.yu@emory.edu

Liang Zhao

Department of Computer Science
Emory University
Atlanta, USA
liang.zhao@emory.edu

ABSTRACT

Deploying Large Language Models (LLMs) for discriminative workloads is often limited by inference latency, compute, and API costs at scale. Active distillation reduces these costs by querying an LLM oracle to train compact discriminative students, but most pipelines distill only final labels, discarding intermediate reasoning signals and offering limited diagnostics of what reasoning is missing and where errors arise. We propose Graph of Concept Predictors (GCP), a reasoning-aware active distillation framework that externalizes the teacher’s decision process as a directed acyclic graph and mirrors it with modular concept predictors in the student. GCP enhances sample efficiency through a graph-aware acquisition strategy that targets uncertainty and disagreement at critical reasoning nodes. Additionally, it improves training stability and efficiency by performing targeted sub-module retraining, which attributes downstream loss to specific concept predictors and updates only the most influential modules. Experiments on eight NLP classification benchmarks demonstrate that GCP enhances performance under limited annotation budgets while yielding more interpretable and controllable training dynamics. Code is available at <https://github.com/Ziyang-Yu/GCP>.

Keywords Active Learning · Knowledge Distillation · Concept-Based Reasoning

1 Introduction

Large Language Models (LLMs) have increasingly been adopted for discriminative tasks such as topic classification, sentiment analysis, stance detection, and clinical risk prediction [1, 2, 3]. Unlike traditional classifiers, which must be retrained whenever the label space or task definition changes, LLMs can generalize to unseen tasks via prompting [4], making them particularly attractive in settings where task definitions evolve rapidly. This flexibility has led to widespread deployment of LLMs as zero-shot or few-shot discriminative models across domains such as finance, healthcare, and large-scale content moderation [5]. However, this capability comes at substantial computational and monetary cost. For example, inference with frontier-scale models can cost on the order of \$5–\$15 per million tokens, and even more efficient offerings such as GPT-4o-mini still incur nontrivial costs when applied to large corpora [6]. For data at scale, such as millions of documents in financial compliance screening, clinical note triage, and e-commerce review classification, the cumulative inference cost and latency quickly become prohibitive, rendering direct LLM deployment impractical for sustained, high-throughput discriminative workloads [7].

A natural solution to these limitations is to distill LLMs into smaller models [8]. Early work has primarily focused on distilling large LLMs into smaller (L)LMs, preserving generative capacity while reducing parameter count [9, 10, 11]. While effective, such approaches remain computationally expensive and often fail to deliver order-of-magnitude savings in inference latency or cost [12]. In contrast, more recent research has demonstrated that distilling LLM behavior into task-specific discriminative models—such as multi-layer perceptrons, linear models, or support vector machines—can yield dramatic efficiency gains, reducing both training and inference costs by orders of magnitude while maintaining strong performance [13, 14]. These approaches typically treat the LLM as an oracle annotator and leverage active learning to minimize the number of LLM queries [15, 16], selecting only the most informative samples for labeling.

The resulting objective is to train a compact discriminative student that approximates the final labels produced by the LLM, achieving substantial financial and time savings suitable for real-world deployment [17].

A key reason LLMs achieve strong performance on complex discriminative tasks is their ability to generate and exploit explicit reasoning processes, such as Chain-of-Thought, Tree-of-Thought, and Graph-of-Thought reasoning [18, 19, 20]. These paradigms can be viewed as structured, directed acyclic graphs of intermediate reasoning states that enable test-time computation scaling and systematic exploration of decision paths, leading to improved accuracy and robustness [21]. A growing body of work has empirically shown that eliciting intermediate reasoning substantially enhances LLM performance, particularly on tasks requiring compositional or multi-factor judgment [18, 22]. Despite this, existing distillation pipelines largely discard these intermediate reasoning signals, training student models solely on final outputs in an end-to-end fashion [8]. This practice results in sparse supervision, obscures the structure of the decision process, reduces interpretability, and limits the student’s ability to recover the teacher’s reasoning competence, especially when distilled into simple discriminative architectures [13].

To approach teacher-level performance, a compact discriminative model must learn not only what prediction to make, but how to arrive at it [18]. This motivates distilling the reasoning process itself, rather than only final labels. However, incorporating reasoning supervision fundamentally complicates the active distillation pipeline. For sample selection, reasoning introduces structured, multi-step dependencies: different examples may expose weaknesses in different parts of the reasoning process, making it insufficient to rely on flat uncertainty or diversity criteria defined only on final predictions [18, 19]. Selecting samples that improve reasoning fidelity requires understanding where in the reasoning process the student deviates from the teacher. For model retraining, reasoning supervision implies that errors are localized to specific intermediate components rather than the final output alone, raising the challenge of how to attribute downstream loss to internal decision modules and update them efficiently without retraining the entire model [23]. These challenges affect both the efficiency and stability of active distillation when reasoning is taken seriously.

To address these challenges, we propose the Graph of Concept Predictors (GCP) framework, a reasoning-aware active distillation approach for compact discriminative models. As is shown in Figure 1, GCP explicitly represents the teacher’s reasoning process as a structured, directed acyclic graph and uses it to guide both sample selection and model retraining. To address the sample selection challenge, GCP prioritizes data points that expose high disagreement and uncertainty on graph-level predictions, rather than relying solely on final-output uncertainty, ensuring that selected samples improve the student’s reasoning fidelity. To handle the retraining challenge, GCP decomposes the student model into modular sub-components aligned with reasoning stages and performs targeted retraining on the modules most responsible for downstream errors. This design enables dense, interpretable supervision of reasoning while preserving the efficiency advantages of small discriminative models, making reasoning-aware distillation practical at scale.

We summarize our main contributions as follows:

- We propose **GCP**, an **active distillation** framework that mirrors a teacher’s reasoning graph with a learnable **Graph of Concept Predictors**, enabling structured and interpretable reasoning transfer.
- We design a **graph-aware acquisition strategy** that prioritizes samples informative for learning concept dependencies and their downstream effects.
- We introduce a **sub-module retraining** strategy that selectively updates the most influential concept predictors while keeping other modules fixed.
- We conduct **extensive experiments** on eight NLP classification benchmarks, demonstrating that GCP achieves stronger performance under limited annotation budgets with more stable and interpretable training dynamics.

2 Related Works

2.1 Concept-Based Reasoning

Concept-based reasoning introduces human-interpretable intermediate variables (“concepts”) to improve transparency and enable test-time interventions. A canonical approach is the Concept Bottleneck Model (CBM), which predicts concepts from inputs and then predicts labels from concepts, enabling concept-level inspection and correction [24]. Recent work extends CBMs under practical constraints: Energy-Based CBMs unify prediction, concept intervention, and conditional interpretation via a joint energy formulation [25], while semi-supervised CBMs reduce concept-labeling cost by leveraging unlabeled data with pseudo-labeling and alignment strategies [26]. Moving beyond i.i.d. concept vectors, Relational CBMs handle relational structure [27], and Graph CBMs learn latent concept graphs to model concept dependencies, improving interventions and interpretability [28].

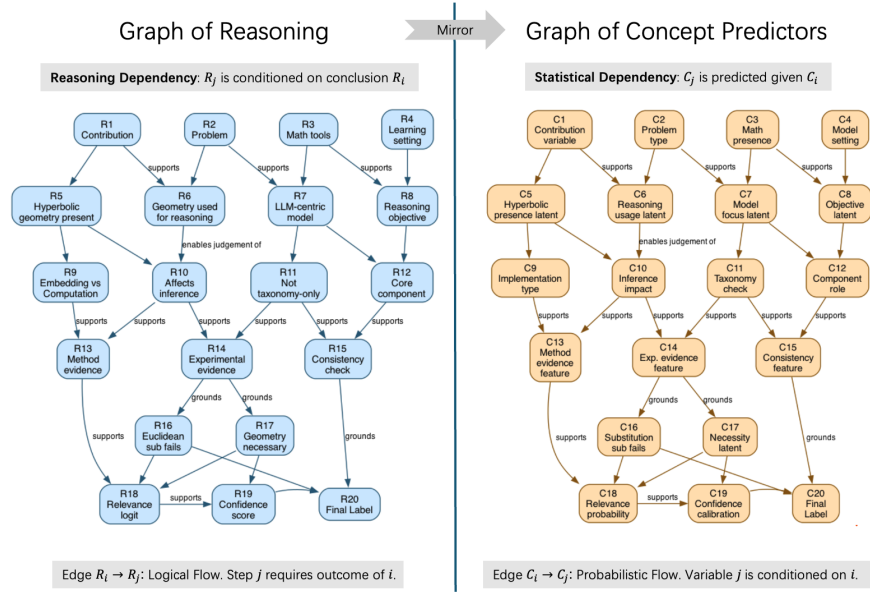


Figure 1: **Mirror mapping from a teacher’s reasoning DAG to a probabilistic Graph of Concept Predictors for classifying whether a paper belongs to Hyperbolic Reasoning in LLMs.** Left: logical dependencies among intermediate conclusions. Right: corresponding concept variables and latent features with conditional links.

In parallel, reasoning-centric approaches in NLP popularize intermediate rationales (e.g., *Chain-of-Thought*) as a mechanism for improved problem solving and supervision [29]. A growing body of work studies distilling such intermediate reasoning traces into smaller models, including step-by-step distillation that trains students on teacher-generated rationales and answers [30], and decomposition-based prompting frameworks that explicitly split problems into subproblems to guide reasoning [31].

2.2 Large Language Models for Annotation

Recent studies have explored the use of large language models (LLMs) as annotators to reduce human labeling effort. Approaches such as zero-shot [22] or few-shot [1] prompting leverage the strong generalization ability of LLMs to produce pseudo-labels for downstream tasks. Many advanced LLMs, such as GPT-4 [32] and Gemini [33] have shown strong ability in annotation for different tasks, such as text classification and sentiment analysis.

2.3 Active Learning with LLM as Annotator

Active learning (AL) is a classical paradigm for reducing annotation cost by selecting the most informative samples for labeling. Uncertainty-based active learning [34] is proposed to iteratively select unlabeled instances about which the current model is least confident. Embedding-based active learning is proposed to select a representative and diverse subset of unlabeled instances, such as CoreSet [35, 36, 37]. Gradient-based active learning is proposed to prioritize unlabeled instances that induce large gradient norms with respect to model parameters, such as BADGE [38, 39] and Batchald [40, 41].

In the era of Large Language Models, several LLM-based active learning approaches are proposed to mitigate the huge cost of manual annotation. FreeAL [42] is proposed to eliminate the need for training multiple task-specific models during active learning by decoupling sample selection from model retraining. LLMaAA [43] is proposed to leverage large language models as adaptive annotators that replace or augment human labeling in active learning loops.

3 Proposed Method

In this section, we first present an overview of our proposed *GCP* framework. We then introduce the *Graph of Concept Predictors* reasoning model. Next, we proceed to present a novel *graph-aware acquisition* strategy for sample selection. Lastly, we present a targeted *sub-module retraining* method.

3.1 GCP Framework

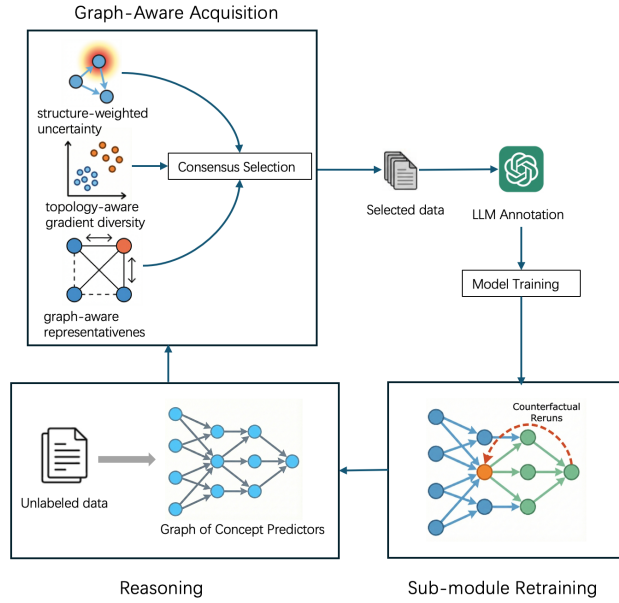


Figure 2: **Overview of our proposed GCP framework (loop view).** The left below part shows concept-level reasoning, where unlabeled inputs are processed by a learned Graph of Concept Predictors that explicitly models dependencies among concepts. The top part illustrates graph-aware acquisition, in which structure-weighted uncertainty, topology-aware gradient diversity, and graph-aware representativeness are jointly evaluated and combined through consensus selection to identify informative samples for LLM annotation. The right below part depicts sub-module retraining, where counterfactual reruns of the GCP attribute errors to individual concept predictors, enabling targeted retraining of high-impact sub-modules for more efficient learning.

We propose *GCP*, a graph-structured active distillation framework that integrates concept-based reasoning, graph-aware sample acquisition, and targeted sub-module retraining in a unified closed-loop pipeline. An overview of the framework is illustrated in Figure 2.

Given an unlabeled data pool \mathcal{U} , we first construct a *Graph of Concept Predictors (GCP)* that decomposes the reasoning process into a directed acyclic graph of concept nodes. Each node represents an intermediate reasoning state, while directed edges encode semantic and causal dependencies between concepts. A forward pass over the GCP produces both concept-level distributions and the final task prediction.

At each active learning iteration, we perform *graph-aware acquisition* over the unlabeled pool. Rather than relying solely on output uncertainty, we evaluate each candidate sample using concept-level signals induced by the GCP, including structure-weighted uncertainty propagation, topology-aware gradient diversity, and graph-based representativeness. These criteria are combined via a consensus-based selection rule to identify a compact yet informative batch of samples for annotation.

Selected samples are then annotated by a large language model (LLM), which provides both final labels and concept-level supervision. The annotated data are used to update the model parameters, after which we invoke a *sub-module retraining* step. Instead of retraining the entire network, we identify concept predictors whose errors most strongly influence the final task loss using counterfactual reruns on the GCP. Only high-impact sub-modules are selectively refined, leading to efficient and stable performance improvements.

This iterative process continues until the annotation budget is exhausted or the convergence criteria are met. By explicitly aligning active learning, distillation, and retraining with the concept graph structure, GCP enables principled reasoning-aware optimization while significantly reducing annotation and computation costs.

3.2 Graph of Concept Predictors

In this section, we introduce **Graph of Concept Predictors (GCP)**, a structured reasoning framework that models reasoning explicitly as a *directed acyclic graph (DAG) of concepts*. Unlike standard neural models that encode reasoning

implicitly in hidden activations [44], GCP represents intermediate reasoning states as explicit *concept nodes* and models their dependencies via learnable transition functions over the graph.

Graph Construction. The concept graph is constructed automatically by an LLM with zero human labeling effort. Given the task definition and a small set of in-context examples, the LLM is prompted *once per task* to decompose the prediction target into an ordered sequence of intermediate conclusions, each accompanied by explicit citations of the conclusions it logically depends on. This single inference call drives a three-stage pipeline: **(i) Decomposition** — the LLM enumerates the intermediate reasoning steps required to reach the final label, producing each step as a discrete conclusion together with the subset of prior conclusions it requires; **(ii) Graph parsing** — each conclusion is instantiated as a node and each cited dependency is instantiated as a directed edge, yielding a candidate directed graph; **(iii) Acyclicity verification** — a topological sort is applied to the candidate graph, and any edges that would introduce a cycle are pruned, guaranteeing a valid DAG. The entire procedure runs once at negligible cost and requires no manual annotation. Importantly, GCP does not assume a *perfect* graph: every concept predictor is a learnable MLP whose parameters are updated during training, so the model can naturally down-weight spurious edges; moreover, the sub-module retraining step (Section 3.4) identifies and corrects weak nodes post hoc. Complete graph examples for two tasks are shown in Figures 2 and 3; the graphs for the remaining six datasets are provided in Appendix 8.

Concept Propagation. Each concept node i is associated with a continuous embedding $h_i \in \mathbb{R}^d$. For input node with no parents, embeddings are obtained directly from the input text x via a learnable encoder:

$$h_0 = f_0(x)$$

For all non-root nodes, concept representations are computed by propagating information from their parent concepts through a node-specific transition function:

$$h_j = f_j(\text{concat}(\{h_i \mid i \in \text{Pa}(j)\}))$$

, where $\text{Pa}(j)$ denotes the parent set of node j in the concept DAG and $\text{concat}(\cdot)$ concatenates parent embeddings along the feature dimension. The output of the final node is the task prediction.

Relation to Structured Reasoning. GCP involves common structured reasoning paradigms: chain-of-thought corresponds to a single path, and tree-based reasoning to branching structures. By allowing multiple reasoning paths to be composed and merged within a DAG, GCP provides a more expressive abstraction while retaining explicit intermediate concept states.

Our analysis shows that explicitly modeling concept dependencies is not merely an architectural choice, but yields fundamental benefits. First, GCP enjoys a strict performance advantage over flat CBMs and end-to-end MLPs when the data-generating process exhibits nontrivial concept dependencies, leading to strictly lower optimal risk under correct factorization. Second, the structured decomposition of GCP induces improved curvature in the optimization landscape, resulting in faster linear convergence for first-order methods. Together, these results establish GCP as statistically and computationally superior with reasoning structure.

3.3 Graph-Aware Acquisition

We propose a *graph-aware acquisition* strategy for concept-guided active learning. Given an unlabeled pool \mathcal{U} , we score each candidate by jointly leveraging (i) structure-weighted uncertainty, (ii) topology-aware gradient diversity, and (iii) graph-aware representativeness. Three acquisition functions are instantiated and then combined via a consensus rule.

Structure-Weighted Uncertainty. For input x and concept node $i \in \mathcal{V}$, let $p_i(x) = (p_{i,0}, \dots, p_{i,d-1})$ denote the predicted concept distribution. Define node-wise entropy as

$$H_i(x) = - \sum_{k=1}^d p_{i,k}(x) \log p_{i,k}(x).$$

We weight nodes by degree centrality

$$w_i = \frac{\text{deg}(i)}{\sum_{j \in \mathcal{V}} \text{deg}(j)}$$

and define the structure-weighted uncertainty score

$$E_{\text{unc}}(x) = \left(\sum_{i \in \mathcal{V}} w_i H_i(x)^p \right)^{1/p}, \quad p \geq 1.$$

The uncertainty-based batch $\mathcal{S}_k^{\text{SWU}}$ is formed by selecting the top- k samples with largest $E_{\text{unc}}(x)$:

$$\mathcal{S}_k^{\text{SWU}} = \text{Top-}k_{x \in \mathcal{U}} E_{\text{unc}}(x)$$

Topology-Aware Gradient Diversity. To encourage diversity, we compare samples using gradients aligned with the shared concept topology. Let $z_i(x)$ denote the gradient of the loss w.r.t. model parameters at node i for sample x . The topology-aware gradient distance is

$$D_{\text{grad}}(x, y) = \left(\sum_{i \in \mathcal{V}} w_i \|z_i(x) - z_i(y)\|_2^p \right)^{1/p}$$

We cluster \mathcal{U} into k groups using D_{grad} and select one medoid per cluster, yielding $\mathcal{S}_k^{\text{grad}}$.

Graph-Aware Representativeness. Each sample x is represented by graph-aligned embeddings $h(x) = \{h_i(x)\}_{i \in \mathcal{V}}$. We measure dissimilarity via a topology-weighted KL divergence:

$$D_{\text{KL}}(x, y) = \sum_{i \in \mathcal{V}} w_i \text{KL}(h_i(x) \| h_i(y))$$

To ensure coverage, we adopt a core-set objective

$$\mathcal{S}_k^{\text{cover}} = \arg \max_{|S|=k} \min_{x \in \mathcal{U}} \min_{y \in \mathcal{L} \cup \mathcal{S}} D_{\text{KL}}(x, y)$$

, which we approximate via clustering in the graph-aware embedding space.

Consensus-Based Selection. We select samples that are simultaneously uncertain, diverse, and representative by intersecting the three candidate sets:

$$\mathcal{S}^* = \mathcal{S}_k^{\text{SWU}} \cap \mathcal{S}_k^{\text{grad}} \cap \mathcal{S}_k^{\text{cover}}$$

This conservative consensus rule yields stable and informative acquisitions under the shared concept graph.

Let B denote the annotation budget per acquisition round. We compute $\mathcal{S}_k^{\text{SWU}}$, $\mathcal{S}_k^{\text{grad}}$, and $\mathcal{S}_k^{\text{cover}}$, and take their intersection \mathcal{S}^* . If $|\mathcal{S}^*| < B$, we fill the remaining slots by adding samples from the union $\mathcal{S}_k^{\text{SWU}} \cup \mathcal{S}_k^{\text{grad}} \cup \mathcal{S}_k^{\text{cover}}$ according to a tie-breaking score (e.g., $E_{\text{unc}}(x)$), until B samples are selected.

3.4 Sub-module Retraining

After concepts and final labels are annotated by the oracle and the student is trained on the annotated data, we perform targeted *sub-module retraining* to further improve the end-task objective. Rather than retraining all concept predictors, we identify the node-level MLPs that contribute most to the final loss and selectively update only these bottleneck modules. As is shown in Figure 3, we observe that even when the model already predicts the correct label, the underlying evidence-related sub-modules can remain poorly calibrated—yielding low confidence and high loss. Retraining only the responsible sub-modules corrects these internal failures and improves confidence and likelihood without unnecessary compute. The sub-module retraining algorithm is shown in Algorithm 1.

Optimization objective. Consider a node $i \in \mathcal{V}$ with parent set $\text{pa}(i)$. To quantify how much the error at node i contributes to the *final* task objective and remove the effect of error propagation from its parents, we evaluate the impact of counterfactual interventions on the concept DAG.

Let $\mathcal{G} = (\mathcal{V}, \mathcal{E})$ be a Graph of Concept Predictors, where each node $j \in \mathcal{V}$ is associated with a concept predictor f_j producing a concept representation h_j . For an intervention set $S \subseteq \mathcal{V}$, we define a counterfactual rerun of the DAG by replacing the concepts of nodes in S with their ground-truth values and recomputing all descendant nodes in topological order. Formally, the intervened concepts $\tilde{\mathbf{h}}^{\text{do}(S)}(x) = \{\tilde{h}_j^{\text{do}(S)}(x)\}_{j \in \mathcal{V}}$ are given by

$$\tilde{h}_j^{\text{do}(S)}(x) = \begin{cases} h_j^*(x), & j \in S, \\ f_j(x, \{\tilde{h}_k^{\text{do}(S)}(x)\}_{k \in \text{pa}(j)}), & j \notin S, \end{cases}$$

where $h_j^*(x)$ denotes the ground-truth concept for node j . Let g denote the final prediction head and $\ell(\cdot, \cdot)$ the downstream task loss. The final loss under intervention S is

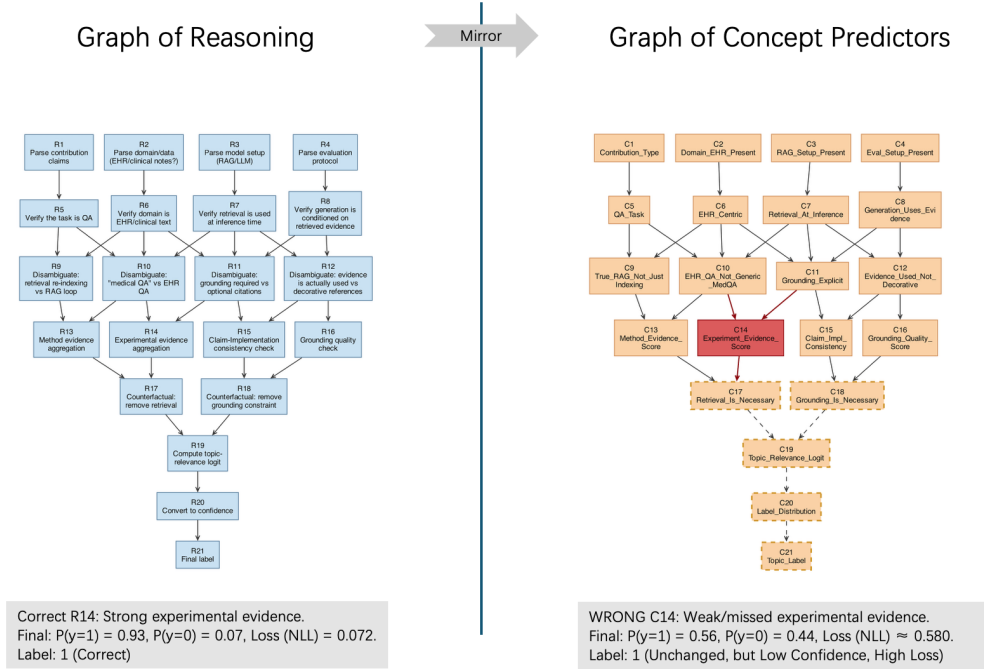


Figure 3: **Mirror-structured reasoning and concept graphs for classifying whether a paper belongs to RAG for EHR Question Answering with grounded clinical evidence.** Both predict the same label, but weaker internal evidence on the right yields lower confidence and higher loss.

$$\mathcal{L}^{\text{do}(S)}(x) = \ell\left(g\left(x, \tilde{\mathbf{h}}^{\text{do}(S)}(x)\right), y\right)$$

We consider two specific interventions. In the *parent-corrected* rerun, we intervene on the parent set $\text{pa}(i)$, yielding the loss $\mathcal{L}_i^{\text{pa}}(x) = \mathcal{L}^{\text{do}(\text{pa}(i))}(x)$. In the *parent+node-corrected* rerun, we additionally intervene on node i , yielding $\mathcal{L}_i^{\text{pa}+i}(x) = \mathcal{L}^{\text{do}(\text{pa}(i) \cup \{i\})}(x)$. We define

$$\Delta_i = \mathbb{E}_x \left[\mathcal{L}_i^{\text{pa}}(x) - \mathcal{L}_i^{\text{pa}+i}(x) \right]$$

, which measures the expected reduction in final loss achieved by correcting node i after its parents have already been corrected. A larger Δ_i indicates that predictor f_i is a more severe bottleneck in the reasoning graph.

This naturally yields the selection objective

$$\mathcal{M}^* = \arg \max_{\mathcal{M} \subseteq \mathcal{V}, |\mathcal{M}|=b} \sum_{i \in \mathcal{M}} \Delta_i$$

i.e., selecting the b concept modules whose correction is expected to yield the largest reduction in the final task loss and therefore should be prioritized for retraining.

Algorithmic selection. We estimate Δ_i by averaging the counterfactual loss difference over the annotated dataset, rank all nodes by Δ_i , and select the top candidates for retraining while freezing the rest.

LLM-guided parent-child regeneration. For each selected node i , we further augment retraining data at the concept level. Conditioning on the semantic definitions of $\text{pa}(i)$ and i , an LLM generates additional valid parent-child concept pairs $\{(h_{\text{pa}(i)}^{(k)}, h_i^{(k)})\}_{k=1}^K$, which are combined with annotated data to retrain f_i .

3.5 Theoretical Analysis

Here, we present a theoretical analysis of the proposed Graph of Concept Predictors (GCP), covering: (i) its performance advantage, (ii) a faster linear convergence guarantee relative to MLPs and CBMs, (iii) the optimality of targeted submodule retraining, and (iv) the associated time-complexity analysis. The detailed proof is provided in Section 7.

Algorithm 1 Sub-module Retraining via Counterfactual Reruns

Input: GCP DAG $\mathcal{G} = (\mathcal{V}, \mathcal{E})$ with predictors $\{f_i\}$; annotated dataset $\mathcal{D} = \{(x, \mathbf{h}, y)\}$; final loss \mathcal{L} ; retrain budget b

Output: Updated predictors $\{f_i\}_{i \in \mathcal{V}}$

Initialize $\Delta_i \leftarrow 0$ for all $i \in \mathcal{V}$

for each $(x, \mathbf{h}, y) \in \mathcal{D}$ **do**

for each node $i \in \mathcal{V}$ **do**

$\mathcal{L}_i^{\text{pa}}(x) \leftarrow \ell\left(g\left(x, \tilde{\mathbf{h}}^{\text{do}(\text{pa}(i))}(x)\right), y\right)$ {substitute h_j^* for all $j \in \text{pa}(i)$ }

$\mathcal{L}_i^{\text{pa}+i}(x) \leftarrow \ell\left(g\left(x, \tilde{\mathbf{h}}^{\text{do}(\text{pa}(i) \cup \{i\})}(x)\right), y\right)$ {substitute h_j^* for all $j \in \text{pa}(i) \cup \{i\}$ }

$\Delta_i \leftarrow \Delta_i + \mathcal{L}_i^{\text{pa}}(x) - \mathcal{L}_i^{\text{pa}+i}(x)$

end for

end for

$\Delta_i \leftarrow \Delta_i / |\mathcal{D}|$ for all $i \in \mathcal{V}$

Select $\mathcal{M}_{\text{retrain}} \leftarrow \text{Top}(\{\Delta_i\}_{i \in \mathcal{V}}, b)$ and freeze f_j for $j \notin \mathcal{M}_{\text{retrain}}$

for each $i \in \mathcal{M}_{\text{retrain}}$ **do**

 Generate additional parent–child concept pairs $(h_{\text{pa}(i)}, h_i)$ using LLM

 Retrain f_i using generated pairs

end for

Performance Advantage of GCP. Our first theorem proves GCP is strictly more expressive, achieving lower Bayes risk than CBM and MLP whenever any concepts remain conditionally dependent given x .

Theorem 3.1 (Strict performance advantage of GCP) *Let $G = (V, E)$ be a directed acyclic graph (DAG) over $V = \{c_1, \dots, c_K, y\}$. Assume the data-generating distribution admits a DAG factorization $p^*(y, \mathbf{c} | x) = \prod_{j=1}^K p^*(c_j | x, \mathbf{c}_{\text{pa}^*(c_j)}) \cdot p^*(y | x, \mathbf{c}_{\text{pa}^*(y)})$. If there exist $i \neq j$ such that $c_i \not\perp\!\!\!\perp c_j | x$ under p^* , then*

$$\mathcal{R}(\mathcal{P}_{\text{GCP}}) < \mathcal{R}(\mathcal{P}_{\text{CBM}}) \leq \mathcal{R}(\mathcal{P}_{\text{MLP}})$$

,where \mathcal{P}_{GCP} consist of all models that factorize according to an arbitrary DAG over concepts and label; \mathcal{P}_{CBM} consist of flat concept bottleneck models that assume conditional independence of concepts given x ; and \mathcal{P}_{MLP} consist of unconstrained predictors $p(y | x)$ without explicit concepts.

Linear Convergence Rate of GCP. We show that the factorized training objective induced by the concept graph admits improved optimization geometry compared with CBM and MLP.

Theorem 3.2 (Faster linear convergence of GCP) *Let $\theta = \{\theta_v\}_{v \in V}$ denote the collection of node-specific parameters in GCP, and define the objective $F(\theta) = \sum_{v \in V} \lambda_v \mathbb{E}[-\log p(v | x, \mathbf{c}_{\text{pa}(v)}; \theta_v)]$. Assume each node-level loss is L_v -smooth and satisfies a local Polyak–Łojasiewicz inequality with constant μ_v . Then F satisfies a local PL inequality with $\mu_{\text{GCP}} = \min_{v \in V} \mu_v$ and gradient descent with step size $1/L$ satisfies*

$$\|\theta_t - \theta^*\| \leq \left(1 - \frac{\mu_{\text{GCP}}}{L}\right)^t \|\theta_0 - \theta^*\|.$$

Moreover, when concept dependencies are explicitly modeled, conditioning on $\mathbf{c}_{\text{pa}(v)}$ yields strictly larger μ_v than marginal predictors, implying $\mu_{\text{GCP}} > \mu_{\text{CBM}} > \mu_{\text{MLP}}$.

Optimality of Sub-Module Retraining. We formalize sub-module retraining as a top- K selection problem under an additive counterfactual utility and show that our algorithm can achieve optimal solution.

Theorem 3.3 (Optimality of Top- K Selection) *Define the empirical counterfactual score used for retraining selection as $\hat{\Delta}_i = \frac{1}{|\mathcal{D}|} \sum_{(x, \mathbf{h}, y) \in \mathcal{D}} (\mathcal{L}_i^{\text{pa}}(x) - \mathcal{L}_i^{\text{pa}+i}(x))$, Rewrite the selection problem as*

$$\max_{S \subseteq \mathcal{V}, |S|=K} \sum_{i \in S} \hat{\Delta}_i. \quad (1)$$

Our algorithm selecting the K nodes with the largest values of $\hat{\Delta}_i$ yields a globally optimal solution to Eq. (1).

Computational Complexity Analysis of Algorithm 1. We analyze the worst-case time complexity of the sub-module retraining procedure, including counterfactual loss evaluation and node selection.

Theorem 3.4 *For a dataset of size N and a concept graph with $|V|$ nodes, the Algorithm 1 worst-case time complexity is $O(N|V|^2)$.*

4 Experiment

In this section, we evaluate our proposed framework on 8 real-world benchmarks against 8 active learning acquisition strategies.

4.1 Experiment Settings

Datasets Details We provide more detailed descriptions of the datasets used in our experiments. We include a detailed introduction and sources as follows:

- **AG News** [45] is a topic classification dataset constructed from news articles collected by the AG corpus. Each instance consists of a news headline and short description, and the task is to classify the article into one of four predefined categories: *World*, *Sports*, *Business*, or *Science/Technology*, forming a standard single-label multi-class text classification problem.
- **Amazon Reviews** [46] is a sentiment classification dataset derived from user-written product reviews on Amazon. Each instance corresponds to a review text associated with a product, and the task is to predict the sentiment polarity expressed in the review, typically formulated as a binary or multi-class classification problem based on review ratings.
- **IMDB Movie Reviews** [47] is a benchmark sentiment analysis dataset consisting of movie reviews written by users on the Internet Movie Database. Each instance contains a single review document, and the task is to classify the sentiment of the review as *positive* or *negative*, resulting in a binary text classification problem.
- **Yelp Reviews** [45] is a large-scale sentiment classification dataset composed of user reviews of businesses on Yelp. Each instance consists of a review text, and the task is to predict the associated star rating or sentiment polarity, typically formulated as a multi-class or binary classification problem depending on the evaluation setting.
- **MNLI (Multi-Genre Natural Language Inference)** [48] is a large-scale natural language inference dataset covering multiple text genres. Each instance consists of a pair of sentences, referred to as a *premise* and a *hypothesis*. The task is to classify the semantic relationship between the two sentences into one of three categories: entailment, contradiction, or neutral.
- **GoEmotions** [49] is a fine-grained emotion classification dataset consisting of short, user-generated texts annotated with emotions. Each instance corresponds to a single sentence, and the task is to predict one or more emotion labels from a set of 27 predefined categories, resulting in a multi-label classification problem with substantial subjectivity and label overlap.
- **SemEval Stance Detection** [50] is a target-dependent stance classification dataset introduced in the SemEval shared tasks. Each instance consists of a text snippet paired with a specific target entity or topic, and the task is to determine the stance expressed in the text toward the given target, classified as *favor*, *against*, or *neutral*.
- **MIMIC-III Clinical Notes** [51] is a large-scale clinical text corpus derived from electronic health records in intensive care units. We consider text classification tasks based on clinical notes, such as discharge summaries, where each instance corresponds to a patient-level clinical document and the task is to predict clinical outcomes or phenotypes (e.g., mortality or disease presence), formulated as binary or multi-label classification problems.

Table 1: Summary of dataset statistics.

Dataset	# Instances	# Classes	Avg. Length	Task Type
AG News	120,000	4	38	Topic
Amazon Reviews	3,000,000	2	90	Sentiment
IMDB	50,000	2	230	Sentiment
Yelp Reviews	560,000	5	150	Sentiment
MNLI	433,000	3	33	NLI
GoEmotions	58,000	27	30	Emotion
SemEval Stance	4,800	3	25	Stance
MIMIC-III (In-hospital Mortality)	50,000	2	1,200	Clinical

The detailed information such as statistics of these datasets is summarized in Table 1.

Evaluation Metric We evaluate performance using test-set accuracy computed from the student model’s final predictions. For single-label classification datasets (MNLI, SemEval, AG News, Amazon, IMDB, Yelp), accuracy is the fraction of examples whose predicted label matches the ground truth. For GoEmotions (multi-label), we binarize each label (e.g., thresholding sigmoid outputs) and report example-level accuracy based on exact match of the predicted label set. For MIMIC-III, we report patient-level accuracy for the downstream clinical endpoint prediction.

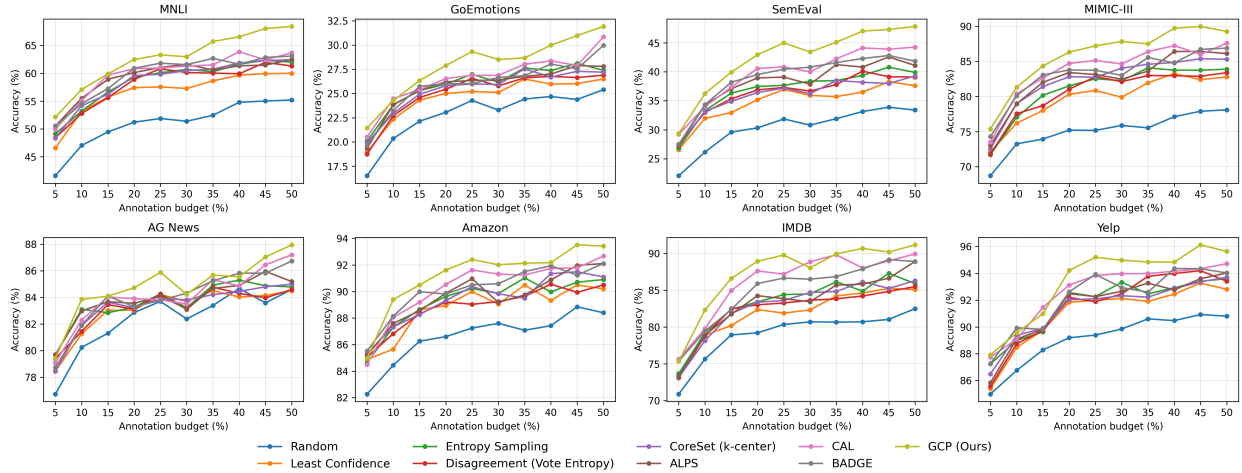


Figure 4: **Performance curves of different sample selection methods for active learning.** The y-axis denotes the accuracy for the classification task, and the x-axis represents the percentage of samples annotated by the LLM for small model training. In this case, 100% denotes that all samples from the training set have been annotated.

Baseline Methods We compare GCP against active learning acquisition strategies. We include widely used uncertainty-based methods—Random sampling, Least Confidence [52], Entropy Sampling [53], and Disagreement (Vote Entropy) [54]—as well as stronger diversity-based and representation-based approaches, including CoreSet (k-center) [35], BADGE [55], ALPS [56], and CAL [57]. These methods select samples based on prediction uncertainty, embedding diversity, or gradient information, but do not exploit explicit concept structure or reasoning dependencies.

Implementation Details We use LLaMA-3-70B as annotator [58]. All experiments are conducted on a single NVIDIA H200 Tensor Core GPU with 141GB HBM3e memory. All models are implemented in PyTorch. We optimize with AdamW using a learning rate of 1×10^{-4} and a batch size of 8, and apply gradient accumulation when needed to maintain stable updates. Unless otherwise stated, each concept predictor is a lightweight MLP with hidden dimension 256 and dropout 0.1. For active learning, we keep the training hyperparameters fixed across rounds and annotation budgets.

LLM Annotation Prompt The following prompt is used when the LLM performs annotation. It instructs the model to jointly predict the classification label and the presence of each concept:

```

You are a precise classifier. Pick exactly one label from the provided label set.
Text: {text}
Label set: {labels}
Moreover, you are a precise concept annotator. Decide if the target concept is
present (1) or absent (0) in the text. Use provided parent concept labels as
hints. Return ONLY the integer 0 or 1.
Parent concept labels: {parent_concept_labels}
Return the result in the following format:
[{"label": 0, "concept": [0, 1, 0, 1, 0]}, {"label": 1, "concept": [1, 0, 1, 0,
1]}, ...]
    
```

4.2 Results and Analysis

This section evaluates the performance of our proposed GCP method compared with other baselines. Performance trends from a 5% to 50% annotating budget are depicted in Figure 4, illustrating the effectiveness of GCP against other baseline methods. Furthermore, we report performance at a 20% GCP annotating budget and other baselines in Table 2.

Overall Performance under Fixed Annotation Budget. As shown in Table 2, GCP delivers the best performance across all eight datasets under a fixed 20% annotation budget, outperforming both uncertainty-based methods and strong gradient/representation baselines. On MNLi, GCP reaches 62.47% accuracy, beating the strongest baseline (BADGE at 60.91%) by +1.56, and on SemEval it improves by +2.38 (42.96% vs. 40.58%). On the clinically complex MIMIC-III task, GCP achieves 86.32%, exceeding CAL (84.71%) by +1.61, highlighting its effectiveness in high-stakes settings.

Table 2: **Baseline comparison under a fixed 20% annotation budget.** All methods are evaluated in a pool-based active learning setting. Best results are in **bold**.

Method	MNLI	GoEmotions	SemEval	MIMIC-III	AG News	Amazon	IMDB	Yelp
Random	51.21	23.06	30.33	75.21	82.87	86.60	79.21	89.19
<i>Classic uncertainty- and diversity-based baselines</i>								
Least Confidence	57.42	25.01	35.18	80.32	83.05	88.94	82.37	91.84
Entropy Sampling	59.30	25.98	37.46	81.51	83.27	89.63	83.41	92.56
Disagreement (Vote Entropy)	58.91	25.44	36.87	81.03	83.11	89.21	83.02	92.19
<i>Representation- and gradient-based strong baselines</i>								
CoreSet (k-center)	59.60	25.80	36.42	82.82	83.23	89.32	83.37	92.03
ALPS	60.12	26.21	38.94	83.41	83.56	89.87	84.26	92.48
CAL	60.83	26.54	40.58	84.71	83.91	90.54	87.62	93.12
BADGE	60.91	26.01	39.53	83.78	83.31	89.81	85.91	92.62
GCP (Ours)	62.47	27.89	42.96	86.32	84.73	91.62	88.94	94.21

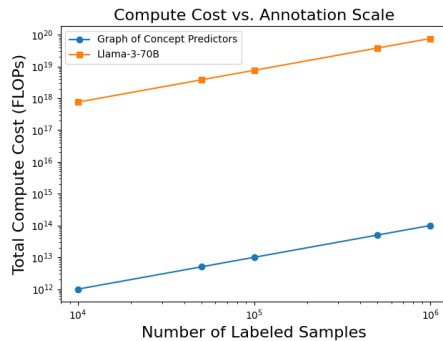


Figure 5: **Compute cost versus annotation scale on a logarithmic axis.** We compare the computational cost between teacher model (Llama-3-70B) versus GCP.

These gains come from our graph-aware acquisition strategy, which selects samples based on their propagated impact over the concept DAG, favoring structurally central concepts and diverse reasoning paths rather than relying on isolated output uncertainty.

Annotation Efficiency and Learning Dynamics. Figure 5 shows that GCP scales far more efficiently than the teacher model (LLaMA-3-70B) as the annotation budget increases. As the number of labeled samples grows from 10^4 to 10^6 , the teacher’s total compute cost rises from approximately 10^{18} to 10^{20} FLOPs, whereas GCP remains in the range of 10^{12} – 10^{14} FLOPs. This corresponds to a consistent $\sim 10^5$ – $10^6\times$ reduction in compute cost across all annotation scales, enabling large-scale annotation and iterative training without prohibitive LLM inference overhead.

Figure 4 shows that GCP delivers faster gains across the full annotation budget range (5%–50%), outperforming competing methods at early, mid, and late active-learning stages. The margin is largest in low-budget settings, where uncertainty-based methods are unstable and gradient-based methods over-focus on local decision boundaries. This stems from the interaction of reasoning-aware acquisition and targeted sub-module retraining: graph-aware selection adds samples that are globally informative with respect to the concept DAG, while counterfactual-guided retraining selectively refines the most influential concept predictors. By avoiding updates to irrelevant modules, GCP stabilizes optimization and translates sparse annotations into sustained improvements, yielding the smooth, consistently superior learning curves observed across datasets.

4.3 Ablation Study

In this section, we conduct ablation studies to quantify the contribution of each component in GCP. Table 3 shows that every design choice matters at a fixed 50% annotation budget: removing any single acquisition signal consistently degrades performance (e.g., w/o SWU reduces MNLI from 68.41 to 66.82 and SemEval from 47.83 to 45.61; w/o Grad

Table 3: **Architecture ablation.** Comparing our proposed GCP with flat CBM (no dependencies) and end-to-end MLP. Performance reported at 50% annotation budget.

Architecture	MNLI	GoEmotions	SemEval	MIMIC-III	AG News	Amazon	IMDB	Yelp
GCP	68.41	31.92	47.83	89.27	87.96	93.42	91.18	95.63
Flat CBM	65.73	30.84	44.26	86.12	87.21	92.67	89.94	94.71
End-to-End MLP	63.18	29.97	41.83	84.03	86.74	92.11	88.92	94.02

Table 4: **Ablation study on major components of GCP.** We report accuracy (%) at 50% annotation budget across 8 datasets. Each row disables one component to assess its contribution. Full model includes all components.

Setting	MNLI	GoEmotions	SemEval	MIMIC-III	AG News	Amazon	IMDB	Yelp
GCP (Full)	68.41	31.92	47.83	89.27	87.96	93.42	91.18	95.63
w/o SWU	66.82	30.74	45.61	87.43	87.21	92.81	90.32	94.91
w/o Grad	66.41	30.28	45.02	87.11	87.08	92.64	89.97	94.74
w/o Coverage	67.02	30.91	46.13	87.86	87.35	92.93	90.51	95.02
w/o Intersection (Union + tie-break)	65.94	30.12	44.58	86.73	86.89	92.41	89.63	94.38
w/o Sub-module Retraining	64.87	29.96	43.21	85.02	86.71	92.18	89.11	94.09

further drops MNLI to 66.41 and SemEval to 45.02), confirming that *structure-weighted uncertainty* and *topology-aware gradient diversity* are both essential for informative acquisition. Table 4 shows that the full GCP model consistently outperforms all ablated variants across datasets. For example, on MNLI, the full model reaches 68.41, compared to 65.94 without intersection and 64.87 without sub-module retraining. On MIMIC-III, accuracy drops from 89.27 (full) to 86.73 when replacing intersection with union and to 85.02 without sub-module retraining. Similar gaps appear on Yelp (95.63 vs. 94.38 and 94.09), demonstrating that each component provides measurable and complementary gains.

Figure 6 shows that sub-module retraining consistently improves the token–accuracy trade-off across all annotation budgets (10–60M): on every dataset, the retraining curve dominates the non-retraining curve. The largest and most persistent gains occur on MNLI/SemEval/MIMIC-III (typically 2–5 points; e.g., at 60M tokens MNLI improves from 63.4 to 68.3 and SemEval from 44.6 to 47.8), with clear improvements also on high-accuracy sentiment/topic tasks (Yelp/Amazon/AG News, typically 1–2 points). Retraining also improves token efficiency, often matching or exceeding no-retraining performance at substantially lower budgets.

Table 5 further disentangles the two key ingredients of GCP’s sub-module retraining: the *targeted selection* of concept predictors and the *LLM-generated supervision*. Removing LLM data while keeping targeted retraining (w/o LLM data) consistently underperforms the full model across all datasets (e.g., MNLI 62.45 vs. 62.81, SemEval 42.75 vs. 43.31), demonstrating that LLM-derived concept annotations provide essential supervision signal. Replacing targeted selection with random node retraining while retaining LLM data (random + LLM data) performs similarly poorly or worse (e.g., SemEval 42.68, Yelp 94.04), confirming that *which* nodes are retrained matters as much as *how* they are supervised. Only the full GCP model, which combines gradient-guided targeted selection with LLM data, achieves the best performance on all eight benchmarks.

5 Conclusion

This paper introduced GCP, an active distillation framework that transfers LLM reasoning into an explicit Graph of Concept Predictors (GCP) for interpretable, concept-level supervision and diagnosis. GCP combines a graph-aware acquisition strategy with a counterfactual sub-module retraining mechanism that selectively updates the most loss-influential concept predictors while keeping others fixed. Experiments across eight benchmarks show consistent gains over strong active learning baselines under limited annotation budgets, and ablations confirm that each component contributes materially to performance.

6 Impact Statement

This work proposes Graph of Concept Predictors (GCP), a reasoning-aware active distillation framework that transfers structured LLM reasoning into compact, interpretable discriminative models. By explicitly modeling intermediate concepts and their dependencies, GCP improves sample efficiency and training stability while substantially reducing compute and inference cost relative to direct LLM deployment.

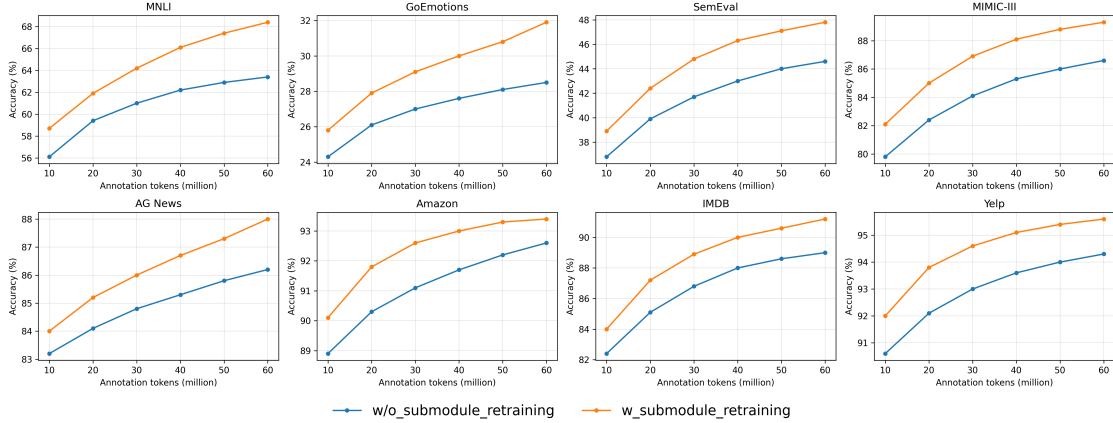


Figure 6: **Ablation Study on targeted sub-module retraining.** The y-axis denotes the accuracy for the classification task, and the x-axis denotes the annotation token usage (in millions).

Table 5: **Ablation on retraining strategy and LLM data.** We compare (a) targeted retraining without LLM data and (b) random node retraining with LLM data against the full GCP model. Accuracy (%) reported at 50% annotation budget.

Method	MNLi	GoEmotions	SemEval	MIMIC-III	AG News	Amazon	IMDB	Yelp
w/o LLM data	62.45	27.93	42.75	86.32	84.73	91.17	88.94	94.21
random + LLM data	62.47	27.89	42.68	86.49	84.97	91.02	88.79	94.04
GCP	62.81	28.23	43.31	86.69	85.12	91.28	89.27	94.53

Broader impacts are positive in high-throughput settings (e.g., content moderation, finance, healthcare triage) where latency, cost, and governance limit frontier-model use: GCP enables cheaper deployment and more transparent diagnostics via concept-level supervision and targeted sub-module retraining. Key risks come from propagating teacher-model biases or errors into concept predictors, but GCP’s modular structure can help localize and correct failures without retraining the full system; it should not be used as a standalone decision-maker in high-stakes contexts.

7 Theoretical Proof

In this section, we provide the formal proof for all the theories presented in the paper.

7.1 Proof of Theorem 3.1

We first show $\mathcal{R}(\mathcal{P}_{\text{CBM}}) \leq \mathcal{R}(\mathcal{P}_{\text{MLP}})$. Given any $p(y | x) \in \mathcal{P}_{\text{MLP}}$, construct a CBM by choosing any concept conditionals $\{p(c_j | x)\}_{j=1}^K$ and setting $p(y | x, \mathbf{c}) \equiv p(y | x)$, which yields the same marginal $p(y | x)$. Hence $\mathcal{P}_{\text{MLP}} \subseteq \mathcal{P}_{\text{CBM}}$ and therefore $\mathcal{R}(\mathcal{P}_{\text{CBM}}) \leq \mathcal{R}(\mathcal{P}_{\text{MLP}})$.

Next, we show $\mathcal{R}(\mathcal{P}_{\text{GCP}}) \leq \mathcal{R}(\mathcal{P}_{\text{CBM}})$. A CBM is a special case of a DAG factorization with $\text{pa}(c_j) = \emptyset$ for all j , so $\mathcal{P}_{\text{CBM}} \subseteq \mathcal{P}_{\text{GCP}}$ and $\mathcal{R}(\mathcal{P}_{\text{GCP}}) \leq \mathcal{R}(\mathcal{P}_{\text{CBM}})$.

It remains to prove strictness: $\mathcal{R}(\mathcal{P}_{\text{GCP}}) < \mathcal{R}(\mathcal{P}_{\text{CBM}})$ when $p^*(\mathbf{c} | x)$ does not factorize.

Fix any CBM p^{CBM} with the constraint $p^{\text{CBM}}(\mathbf{c} | x) = \prod_{j=1}^K p^{\text{CBM}}(c_j | x)$. For each x , let $q_x(\mathbf{c}) := p^*(\mathbf{c} | x)$ and $r_x(\mathbf{c}) := \prod_{j=1}^K p^{\text{CBM}}(c_j | x)$. By assumption, there exist $i \neq j$ such that $c_i \not\perp c_j | x$ under p^* , hence q_x cannot equal any product-form distribution r_x on a set of x with positive probability. Therefore,

$$\mathbb{E}_{p^*(x)} [\text{KL}(q_x || r_x)] > 0.$$

Now consider the following GCP model constructed directly from p^* : choose a DAG that realizes the factorization of $p^*(y, \mathbf{c} | x)$ and set each conditional in the GCP equal to the corresponding true conditional, so that the resulting GCP marginal satisfies $p^{\text{GCP}}(y | x) = p^*(y | x)$. Hence $\mathcal{R}(\mathcal{P}_{\text{GCP}}) = \mathbb{E}_{p^*(x,y)} [-\log p^*(y | x)]$.

For any CBM, the mismatch in the constrained concept distribution implies the joint (y, \mathbf{c}) conditional is misspecified, and by the KL chain rule,

$$\mathbb{E}_{p^*(x)} [\text{KL}(p^*(y, \mathbf{c} | x) \| p^{\text{CBM}}(y, \mathbf{c} | x))] = \mathbb{E}_{p^*(x)} [\text{KL}(p^*(\mathbf{c} | x) \| p^{\text{CBM}}(\mathbf{c} | x))] + \mathbb{E}_{p^*(x, \mathbf{c})} [\text{KL}(p^*(y | x, \mathbf{c}) \| p^{\text{CBM}}(y | x, \mathbf{c}))] > 0$$

Since marginalization cannot increase KL divergence,

$$\mathbb{E}_{p^*(x)} [\text{KL}(p^*(y | x) \| p^{\text{CBM}}(y | x))] > 0,$$

which is equivalent to a strictly positive excess cross-entropy (negative log-likelihood) risk compared with $p^*(y | x)$. Therefore $\mathcal{R}(\mathcal{P}_{\text{GCP}}) < \mathcal{R}(\mathcal{P}_{\text{CBM}})$, completing the proof.

7.2 Proof of Theorem 3.2

Step 1: PL for the sum objective. Since $F(\theta) = \sum_{v \in V} \lambda_v F_v(\theta_v)$ is block-separable in θ , its gradient satisfies

$$\|\nabla F(\theta)\|^2 = \sum_{v \in V} \|\lambda_v \nabla F_v(\theta_v)\|^2 \geq \left(\min_{v \in V} \lambda_v^2 \right) \sum_{v \in V} \|\nabla F_v(\theta_v)\|^2.$$

By the node-level PL inequalities,

$$\|\nabla F_v(\theta_v)\|^2 \geq 2\mu_v (F_v(\theta_v) - F_v(\theta_v^*)).$$

Combining and using $\mu_{\text{GCP}} = \min_v \mu_v$ gives (up to constant rescaling absorbed into μ_{GCP} by the fixed weights $\{\lambda_v\}$)

$$\frac{1}{2} \|\nabla F(\theta)\|^2 \geq \mu_{\text{GCP}} (F(\theta) - F(\theta^*))$$

locally, i.e., F satisfies a local PL inequality.

Step 2: Smooth PL \Rightarrow linear convergence. Under L -smoothness, standard descent analysis with step size $1/L$ yields

$$F(\theta_{t+1}) - F(\theta^*) \leq \left(1 - \frac{\mu_{\text{GCP}}}{L}\right) (F(\theta_t) - F(\theta^*)),$$

and iterating gives the stated linear rate in function value. A local error bound (or quadratic growth) implied by PL yields the stated contraction in parameter distance.

Step 3: Comparing $\mu_{\text{GCP}}, \mu_{\text{CBM}}, \mu_{\text{MLP}}$. When dependencies are omitted (CBM/MLP), the corresponding objectives remove conditioning variables and effectively drop edge-induced terms, which reduces local curvature and hence decreases the best achievable PL constants. If at least one modeled dependency contributes nonzero additional curvature, then the resulting PL constant is strictly larger, implying $\mu_{\text{GCP}} > \mu_{\text{CBM}} > \mu_{\text{MLP}}$.

7.3 Proof of Theorem 3.3

Let $\{\widehat{\Delta}_{(1)} \geq \widehat{\Delta}_{(2)} \geq \dots \geq \widehat{\Delta}_{(|V|)}\}$ be the sorted scores, and let S^* be the set of indices of the top- K scores. For any feasible S with $|S| = K$, if $S \neq S^*$, then there exists $i \in S \setminus S^*$ and $j \in S^* \setminus S$ such that $\widehat{\Delta}_j \geq \widehat{\Delta}_i$. Swapping i out and j in does not decrease the objective:

$$\sum_{\ell \in (S \setminus \{i\}) \cup \{j\}} \widehat{\Delta}_\ell = \sum_{\ell \in S} \widehat{\Delta}_\ell - \widehat{\Delta}_i + \widehat{\Delta}_j \geq \sum_{\ell \in S} \widehat{\Delta}_\ell.$$

By repeating this exchange argument finitely many times, any feasible S can be transformed into S^* without decreasing the objective. Hence S^* is globally optimal.

7.4 Proof of Theorem 3.4

In the worst case, Algorithm 1 evaluates (or replays) counterfactual losses for each node and for each example. Let $|V|$ be the number of nodes. For a fixed example, computing node-wise contributions can require propagating information across the graph; under dense connectivity or full pairwise interactions this costs $\mathcal{O}(|V|^2)$ per example. Aggregating over N examples yields $\mathcal{O}(N|V|^2)$ total time in the worst case. Lower-order terms (e.g., sorting $|V|$ scores, $\mathcal{O}(|V| \log |V|)$) are dominated.

8 Concept Graph Examples

To support reproducibility, we provide the LLM-generated concept graphs for all eight datasets used in our experiments. Figures 2 and 3 in the main paper already show two complete examples (AG News and MIMIC-III RAG). The graphs for the remaining six datasets are shown below. Each graph was produced by a single LLM call per task using the following three-step procedure: (i) the LLM was prompted with the task definition and a small set of in-context examples and asked to enumerate the intermediate reasoning conclusions needed to arrive at the final label, together with explicit citations of which prior conclusions each new conclusion depends on; (ii) conclusions were parsed as nodes and cited dependencies as directed edges; (iii) a topological sort was applied and any cycle-inducing edges were pruned to guarantee a valid DAG. No human labeling or graph editing was performed at any stage.

Prompt Template. The prompt used for graph construction follows the template below (angle-bracket placeholders are filled per task):

```
You are given the following classification task: <TASK DEFINITION>.
Here are a few examples: <IN-CONTEXT EXAMPLES>.
Your goal is to decompose the reasoning required to solve this task into an
ordered list of intermediate conclusions.
For each conclusion, specify: (1) a concise label for the concept, and (2)
the indices of any prior conclusions it directly depends on (leave empty if
it depends only on the raw input).
Output each conclusion on a new line in the format: [INDEX] <concept
label> | depends on: [DEPENDENCY INDICES].
The final conclusion should correspond to the prediction target.
```

Graphs for Remaining Datasets. (Placeholder — figures for Amazon Reviews, IMDB, Yelp Reviews, MNLI, GoEmotions, and SemEval Stance Detection to be inserted here in the camera-ready version.)

References

- [1] Tom Brown, Benjamin Mann, Nick Ryder, Melanie Subbiah, Jared D Kaplan, Prafulla Dhariwal, Arvind Nee-lakantan, Pranav Shyam, Girish Sastry, Amanda Askell, et al. Language models are few-shot learners. *Advances in neural information processing systems*, 33:1877–1901, 2020.
- [2] Iain J. Cruickshank and Lynnette Hui Xian Ng. Prompting and fine-tuning open-sourced large language models for stance classification, 2024.
- [3] Mohamed Rezk, Patricia Cabanillas Silva, and Fried-Michael Dahlweid. Llms for clinical risk prediction, 2024.
- [4] Takeshi Kojima, Shixiang Shane Gu, Machel Reid, Yutaka Matsuo, and Yusuke Iwasawa. Large language models are zero-shot reasoners, 2023.
- [5] Humza Naveed, Asad Ullah Khan, Shi Qiu, Muhammad Saqib, Saeed Anwar, Muhammad Usman, Naveed Akhtar, Nick Barnes, and Ajmal Mian. A comprehensive overview of large language models, 2024.
- [6] Mehmet Hamza Erol, Batu El, Mirac Suzgun, Mert Yuksekgonul, and James Zou. Cost-of-pass: An economic framework for evaluating language models, 2025.
- [7] Guangji Bai, Zheng Chai, Chen Ling, Shiyu Wang, Jiaying Lu, Nan Zhang, Tingwei Shi, Ziyang Yu, Mengdan Zhu, Yifei Zhang, Xinyuan Song, Carl Yang, Yue Cheng, and Liang Zhao. Beyond efficiency: A systematic survey of resource-efficient large language models, 2024.
- [8] Geoffrey Hinton. Distilling the knowledge in a neural network. *arXiv preprint arXiv:1503.02531*, 2, 2015.
- [9] Victor Sanh, Lysandre Debut, Julien Chaumond, and Thomas Wolf. Distilbert, a distilled version of bert: smaller, faster, cheaper and lighter, 2020.
- [10] Xiaoqi Jiao, Yichun Yin, Lifeng Shang, Xin Jiang, Xiao Chen, Linlin Li, Fang Wang, and Qun Liu. Tinybert: Distilling bert for natural language understanding, 2020.
- [11] Zhiqing Sun, Hongkun Yu, Xiaodan Song, Renjie Liu, Yiming Yang, and Denny Zhou. Mobilebert: a compact task-agnostic bert for resource-limited devices, 2020.
- [12] Zhongwei Wan, Xin Wang, Che Liu, Samiul Alam, Yu Zheng, Jiachen Liu, Zhongnan Qu, Shen Yan, Yi Zhu, Quanlu Zhang, Mosharaf Chowdhury, and Mi Zhang. Efficient large language models: A survey, 2024.

- [13] Namgyu Ho, Laura Schmid, and Se-Young Yun. Large language models are reasoning teachers, 2023.
- [14] Savita Bhat and Vasudeva Varma. Large language models as annotators: A preliminary evaluation for annotating low-resource language content. In Daniel Deutsch, Rotem Dror, Steffen Eger, Yang Gao, Christoph Leiter, Juri Opitz, and Andreas Rücklé, editors, *Proceedings of the 4th Workshop on Evaluation and Comparison of NLP Systems*, pages 100–107, Bali, Indonesia, November 2023. Association for Computational Linguistics.
- [15] Yu Xia, Subhojyoti Mukherjee, Zhouhang Xie, Junda Wu, Xintong Li, Ryan Aponte, Hanjia Lyu, Joe Barrow, Hongjie Chen, Franck Dernoncourt, Branislav Kveton, Tong Yu, Ruiyi Zhang, Jiuxiang Gu, Nesreen K. Ahmed, Yu Wang, Xiang Chen, Hanieh Deilamsalehy, Sungchul Kim, Zhengmian Hu, Yue Zhao, Nedim Lipka, Seunghyun Yoon, Ting-Hao Kenneth Huang, Zichao Wang, Puneet Mathur, Soumyabrata Pal, Koyel Mukherjee, Zhehao Zhang, Namyong Park, Thien Huu Nguyen, Jiebo Luo, Ryan A. Rossi, and Julian McAuley. From selection to generation: A survey of llm-based active learning, 2025.
- [16] Hui Xiang, Jinqiao Shi, Ting Zhang, Xiaojie Zhao, Yong Liu, and Yong Ma. Promptal: Sample-aware dynamic soft prompts for few-shot active learning, 2025.
- [17] Kumar Shridhar, Alessandro Stolfo, and Mrinmaya Sachan. Distilling reasoning capabilities into smaller language models, 2023.
- [18] Jason Wei, Xuezhi Wang, Dale Schuurmans, et al. Chain-of-thought prompting elicits reasoning in large language models. In *Advances in Neural Information Processing Systems (NeurIPS)*, 2022.
- [19] Shunyu Yao, Dian Yu, Jeffrey Zhao, Izhak Shafran, Thomas L. Griffiths, Yuan Cao, and Karthik Narasimhan. Tree of thoughts: Deliberate problem solving with large language models, 2023.
- [20] Yao Yao, Zuchao Li, and Hai Zhao. Beyond chain-of-thought, effective graph-of-thought reasoning in language models, 2024.
- [21] Chengrun Yang, Xuezhi Wang, Yifeng Lu, Hanxiao Liu, Quoc V. Le, Denny Zhou, and Xinyun Chen. Large language models as optimizers, 2024.
- [22] Takeshi Kojima, Shixiang Shane Gu, Machel Reid, Yutaka Matsuo, and Yusuke Iwasawa. Large language models are zero-shot reasoners. *Advances in neural information processing systems*, 35:22199–22213, 2022.
- [23] Jie Huang and Kevin Chen-Chuan Chang. Towards reasoning in large language models: A survey, 2023.
- [24] Pang Wei Koh, Thao Nguyen, Yew Siang Tang, Stephen Mussmann, Emma Pierson, Been Kim, and Percy Liang. Concept bottleneck models. In *Proceedings of the 37th International Conference on Machine Learning (ICML)*, 2020.
- [25] X. Xu et al. Energy-based concept bottleneck models: Unifying prediction, concept intervention, and conditional interpretation. In *International Conference on Learning Representations (ICLR)*, 2024. arXiv:2401.14142.
- [26] L. Hu et al. Semi-supervised concept bottleneck models. *arXiv preprint arXiv:2406.18992*, 2024.
- [27] Luke Melas-Kyriazi et al. Relational concept bottleneck models. *arXiv preprint arXiv:2308.11991*, 2023.
- [28] Haotian Xu, Tsui-Wei Weng, Lam M. Nguyen, and Tengfei Ma. Graph concept bottleneck models. *arXiv preprint arXiv:2508.14255*, 2025.
- [29] Jason Wei, Xuezhi Wang, Dale Schuurmans, et al. Chain-of-thought prompting elicits reasoning in large language models. In *Advances in Neural Information Processing Systems (NeurIPS)*, 2022.
- [30] Ching-Yao Hsieh et al. Distilling step-by-step: Outperforming larger language models with less training data and smaller model sizes. In *Proceedings of the 61st Annual Meeting of the Association for Computational Linguistics (ACL)*, 2023.
- [31] Mohit Shridhar, Jesse Thomason, Daniel Gordon, et al. Socratic models: Composing zero-shot multimodal reasoning with language. In *International Conference on Learning Representations (ICLR)*, 2023.
- [32] Josh Achiam, Steven Adler, Sandhini Agarwal, Lama Ahmad, Ilge Akkaya, Florencia Leoni Aleman, Diogo Almeida, Janko Altschmidt, Sam Altman, Shyamal Anadkat, et al. Gpt-4 technical report. *arXiv preprint arXiv:2303.08774*, 2023.
- [33] Gemini Team, Rohan Anil, Sebastian Borgeaud, Jean-Baptiste Alayrac, Jiahui Yu, Radu Soriccut, Johan Schalkwyk, Andrew M Dai, Anja Hauth, Katie Millican, et al. Gemini: a family of highly capable multimodal models. *arXiv preprint arXiv:2312.11805*, 2023.
- [34] David D Lewis. A sequential algorithm for training text classifiers: Corrigendum and additional data. In *Acm Sigir Forum*, volume 29, pages 13–19. ACM New York, NY, USA, 1995.
- [35] Ozan Sener and Silvio Savarese. Active learning for convolutional neural networks: A core-set approach. In *International Conference on Learning Representations*, 2018.

- [36] Yonatan Geifman and Ran El-Yaniv. Deep active learning over the long tail. *arXiv preprint arXiv:1711.00941*, 2017.
- [37] Gui Citovsky, Giulia DeSalvo, Claudio Gentile, Lazaros Karydas, Anand Rajagopalan, Afshin Rostamizadeh, and Sanjiv Kumar. Batch active learning at scale. *Advances in Neural Information Processing Systems*, 34:11933–11944, 2021.
- [38] Jordan Ash, Chicheng Zhang, Akshay Krishnamurthy, John Langford, and Alekh Agarwal. Deep batch active learning by diverse, uncertain gradient lower bounds. In *International Conference on Learning Representations*, 2020.
- [39] Jordan Ash, Surbhi Goel, Akshay Krishnamurthy, and Sham Kakade. Gone fishing: Neural active learning with fisher embeddings. *Advances in Neural Information Processing Systems*, 34:8927–8939, 2021.
- [40] Andreas Kirsch, Joost Van Amersfoort, and Yarin Gal. Batchbald: Efficient and diverse batch acquisition for deep bayesian active learning. *Advances in neural information processing systems*, 32, 2019.
- [41] Yarin Gal, Riashat Islam, and Zoubin Ghahramani. Deep bayesian active learning with image data. In *International conference on machine learning*, pages 1183–1192. PMLR, 2017.
- [42] Ruixuan Xiao, Yiwen Dong, Junbo Zhao, Runze Wu, Minmin Lin, Gang Chen, and Haobo Wang. Freeal: Towards human-free active learning in the era of large language models. *arXiv preprint arXiv:2311.15614*, 2023.
- [43] Ruoyu Zhang, Yanzeng Li, Yongliang Ma, Ming Zhou, and Lei Zou. Llmaa: Making large language models as active annotators. *arXiv preprint arXiv:2310.19596*, 2023.
- [44] Ashish Vaswani, Noam Shazeer, Niki Parmar, Jakob Uszkoreit, Llion Jones, Aidan N Gomez, Łukasz Kaiser, and Illia Polosukhin. Attention is all you need. *Advances in neural information processing systems*, 30, 2017.
- [45] Xiang Zhang, Junbo Zhao, and Yann LeCun. Character-level convolutional networks for text classification. *Advances in Neural Information Processing Systems*, 28, 2015.
- [46] Julian McAuley, Christopher Targett, Qinfeng Shi, and Anton van den Hengel. Image-based recommendations on styles and substitutes. In *Proceedings of SIGIR*, 2015.
- [47] Andrew L Maas, Raymond E Daly, Peter T Pham, Dan Huang, Andrew Y Ng, and Christopher Potts. Learning word vectors for sentiment analysis. In *Proceedings of the 49th Annual Meeting of the Association for Computational Linguistics*, pages 142–150, 2011.
- [48] Adina Williams, Nikita Nangia, and Samuel Bowman. A broad-coverage challenge corpus for sentence understanding through inference. In *Proceedings of the 2018 conference of the North American chapter of the association for computational linguistics: human language technologies, volume 1 (long papers)*, pages 1112–1122, 2018.
- [49] Dorottya Demszky, Dana Movshovitz-Attias, Jeongwoo Ko, Alan Cowen, Gaurav Nemade, and Sujith Ravi. Goemotions: A dataset of fine-grained emotions. *arXiv preprint arXiv:2005.00547*, 2020.
- [50] Roberto Navigli et al. Semeval-2017 task 12: Clinical tempeval. In *Proceedings of the International Workshop on Semantic Evaluation (SemEval)*, 2017.
- [51] Alistair E. W. Johnson et al. Mimic-iii, a freely accessible critical care database. *Scientific Data*, 2016.
- [52] Aron Culotta and Andrew McCallum. Reducing labeling effort for structured prediction tasks. In *AAAI*, 2005.
- [53] Claude E. Shannon. A mathematical theory of communication. *Bell System Technical Journal*, 1948.
- [54] Sean P. Engelson and Ido Dagan. The committee machine—a flexible approach to uncertainty in machine learning. In *ICML*, 1996.
- [55] Jordan T Ash, Chicheng Zhang, Akshay Krishnamurthy, John Langford, and Alekh Agarwal. Deep batch active learning by diverse, uncertain gradient lower bounds. *arXiv preprint arXiv:1906.03671*, 2019.
- [56] Michelle Yuan et al. Cold-start active learning through self-supervised language modeling. In *EMNLP*, 2020.
- [57] Katerina Margatina, Giorgos Vernikos, Loïc Barrault, and Nikolaos Aletras. Active learning by acquiring contrastive examples. In *EMNLP*, 2021.
- [58] Aaron Grattafiori, Abhimanyu Dubey, Abhinav Jauhri, Abhinav Pandey, Abhishek Kadian, Ahmad Al-Dahle, Aiesha Letman, Akhil Mathur, Alan Schelten, Alex Vaughan, Amy Yang, Angela Fan, Anirudh Goyal, Anthony Hartshorn, Aobo Yang, Archi Mitra, Archie Sravankumar, Artem Korenev, Arthur Hinsvark, Arun Rao, Aston Zhang, Aurelien Rodriguez, Austen Gregerson, Ava Spataru, Baptiste Roziere, Bethany Biron, Binh Tang, Bobbie Chern, Charlotte Caucheteux, Chaya Nayak, Chloe Bi, Chris Marra, Chris McConnell, Christian Keller, Christophe Touret, Chunyang Wu, Corinne Wong, Cristian Canton Ferrer, Cyrus Nikolaidis, Damien Allonsius, Daniel Song, Danielle Pintz, Danny Livshits, Danny Wyatt, David Esiobu, Dhruv Choudhary, Dhruv Mahajan,

Diego Garcia-Olano, Diego Perino, Dieuwke Hupkes, Egor Lakomkin, Ehab AlBadawy, Elina Lobanova, Emily Dinan, Eric Michael Smith, Filip Radenovic, Francisco Guzmán, Frank Zhang, Gabriel Synnaeve, Gabrielle Lee, Georgia Lewis Anderson, Govind Thattai, Graeme Nail, Gregoire Mialon, Guan Pang, Guillem Cucurell, Hailey Nguyen, Hannah Korevaar, Hu Xu, Hugo Touvron, Iliyan Zarov, Imanol Arrieta Ibarra, Isabel Kloumann, Ishan Misra, Ivan Evtimov, Jack Zhang, Jade Copet, Jaewon Lee, Jan Geffert, Jana Vranes, Jason Park, Jay Mahadeokar, Jeet Shah, Jelmer van der Linde, Jennifer Billock, Jenny Hong, Jenya Lee, Jeremy Fu, Jianfeng Chi, Jianyu Huang, Jiawen Liu, Jie Wang, Jiecao Yu, Joanna Bitton, Joe Spisak, Jongsoo Park, Joseph Rocca, Joshua Johnstun, Joshua Saxe, Junteng Jia, Kalyan Vasuden Alwala, Karthik Prasad, Kartikeya Upasani, Kate Plawiak, Ke Li, Kenneth Heafield, Kevin Stone, Khalid El-Arini, Krithika Iyer, Kshitiz Malik, Kuenley Chiu, Kunal Bhalla, Kushal Lakhotia, Lauren Rantala-Yearly, Laurens van der Maaten, Lawrence Chen, Liang Tan, Liz Jenkins, Louis Martin, Lovish Madaan, Lubo Malo, Lukas Blecher, Lukas Landzaat, Luke de Oliveira, Madeline Muzzi, Mahesh Pasupuleti, Mannat Singh, Manohar Paluri, Marcin Kardas, Maria Tsimpoukelli, Mathew Oldham, Mathieu Rita, Maya Pavlova, Melanie Kambadur, Mike Lewis, Min Si, Mitesh Kumar Singh, Mona Hassan, Naman Goyal, Narjes Torabi, Nikolay Bashlykov, Nikolay Bogoychev, Niladri Chatterji, Ning Zhang, Olivier Duchenne, Onur Çelebi, Patrick Alrassy, Pengchuan Zhang, Pengwei Li, Petar Vasic, Peter Weng, Prajjwal Bhargava, Pratik Dubal, Praveen Krishnan, Punit Singh Koura, Puxin Xu, Qing He, Qingxiao Dong, Ragavan Srinivasan, Raj Ganapathy, Ramon Calderer, Ricardo Silveira Cabral, Robert Stojnic, Roberta Raileanu, Rohan Maheswari, Rohit Girdhar, Rohit Patel, Romain Sauvestre, Ronnie Polidoro, Roshan Sumbaly, Ross Taylor, Ruan Silva, Rui Hou, Rui Wang, Saghar Hosseini, Sahana Chennabasappa, Sanjay Singh, Sean Bell, Seohyun Sonia Kim, Sergey Edunov, Shaoliang Nie, Sharan Narang, Sharath Rapparthi, Sheng Shen, Shengye Wan, Shruti Bhosale, Shun Zhang, Simon Vandenhende, Soumya Batra, Spencer Whitman, Sten Sootla, Stephane Collet, Suchin Gururangan, Sydney Borodinsky, Tamar Herman, Tara Fowler, Tarek Sheasha, Thomas Georgiou, Thomas Scialom, Tobias Speckbacher, Todor Mihaylov, Tong Xiao, Ujjwal Karn, Vedanuj Goswami, Vibhor Gupta, Vignesh Ramanathan, Viktor Kerkez, Vincent Gonguet, Virginie Do, Vish Vogeti, Vítor Albiero, Vladan Petrovic, Weiwei Chu, Wenhan Xiong, Wenyin Fu, Whitney Meers, Xavier Martinet, Xiaodong Wang, Xiaofang Wang, Xiaoqing Ellen Tan, Xide Xia, Xinfeng Xie, Xuchao Jia, Xuwei Wang, Yaelle Goldschlag, Yashesh Gaur, Yasmine Babaei, Yi Wen, Yiwen Song, Yuchen Zhang, Yue Li, Yuning Mao, Zacharie Delpierre Coudert, Zheng Yan, Zhengxing Chen, Zoe Papanikos, Aaditya Singh, Aayushi Srivastava, Abha Jain, Adam Kelsey, Adam Shajnfeld, Adithya Gangidi, Adolfo Victoria, Ahuva Goldstand, Ajay Menon, Ajay Sharma, Alex Boesenberg, Alexei Baevski, Allie Feinstein, Amanda Kallet, Amit Sangani, Amos Teo, Anam Yunus, Andrei Lupu, Andres Alvarado, Andrew Caples, Andrew Gu, Andrew Ho, Andrew Poulton, Andrew Ryan, Ankit Ramchandani, Annie Dong, Annie Franco, Anuj Goyal, Aparajita Saraf, Arkabandhu Chowdhury, Ashley Gabriel, Ashwin Barambe, Assaf Eisenman, Azadeh Yazdan, Beau James, Ben Maurer, Benjamin Leonhardi, Bernie Huang, Beth Loyd, Beto De Paola, Bhargavi Paranjape, Bing Liu, Bo Wu, Boyu Ni, Braden Hancock, Bram Wasti, Brandon Spence, Brani Stojkovic, Brian Gamido, Britt Montalvo, Carl Parker, Carly Burton, Catalina Mejia, Ce Liu, Changan Wang, Changkyu Kim, Chao Zhou, Chester Hu, Ching-Hsiang Chu, Chris Cai, Chris Tindal, Christoph Feichtenhofer, Cynthia Gao, Damon Civin, Dana Beaty, Daniel Kreymer, Daniel Li, David Adkins, David Xu, Davide Testuggine, Delia David, Devi Parikh, Diana Liskovich, Didem Foss, DingKang Wang, Duc Le, Dustin Holland, Edward Dowling, Eissa Jamil, Elaine Montgomery, Eleonora Presani, Emily Hahn, Emily Wood, Eric-Tuan Le, Erik Brinkman, Esteban Arcaute, Evan Dunbar, Evan Smothers, Fei Sun, Felix Kreuk, Feng Tian, Filippos Kokkinos, Firat Ozgenel, Francesco Caggioni, Frank Kanayet, Frank Seide, Gabriela Medina Florez, Gabriella Schwarz, Gada Badeer, Georgia Swee, Gil Halpern, Grant Herman, Grigory Sizov, Guangyi, Zhang, Guna Lakshminarayanan, Hakan Inan, Hamid Shojanazeri, Han Zou, Hannah Wang, Hanwen Zha, Haroun Habeeb, Harrison Rudolph, Helen Suk, Henry Aspegren, Hunter Goldman, Hongyuan Zhan, Ibrahim Damlaj, Igor Molybog, Igor Tufanov, Ilias Leontiadis, Irina-Elena Veliche, Itai Gat, Jake Weissman, James Geboski, James Kohli, Janice Lam, Japhet Asher, Jean-Baptiste Gaya, Jeff Marcus, Jeff Tang, Jennifer Chan, Jenny Zhen, Jeremy Reizenstein, Jeremy Teboul, Jessica Zhong, Jian Jin, Jingyi Yang, Joe Cummings, Jon Carvill, Jon Shepard, Jonathan McPhie, Jonathan Torres, Josh Ginsburg, Junjie Wang, Kai Wu, Kam Hou U, Karan Saxena, Kartikay Khandelwal, Katayoun Zand, Kathy Matosich, Kaushik Veeraraghavan, Kelly Michelena, Keqian Li, Kiran Jagadeesh, Kun Huang, Kunal Chawla, Kyle Huang, Lailin Chen, Lakshya Garg, Lavender A, Leandro Silva, Lee Bell, Lei Zhang, Liangpeng Guo, Licheng Yu, Liron Moshkovich, Luca Wehrstedt, Madian Khabsa, Manav Avalani, Manish Bhatt, Martynas Mankus, Matan Hasson, Matthew Lennie, Matthias Reso, Maxim Groshev, Maxim Naumov, Maya Lathi, Meghan Keneally, Miao Liu, Michael L. Seltzer, Michal Valko, Michelle Restrepo, Mihir Patel, Mik Vyatskov, Mikayel Samvelyan, Mike Clark, Mike Macey, Mike Wang, Miquel Jubert Hermoso, Mo Metanat, Mohammad Rastegari, Munish Bansal, Nandhini Santhanam, Natascha Parks, Natasha White, Navyata Bawa, Nayan Singhal, Nick Egebo, Nicolas Usunier, Nikhil Mehta, Nikolay Pavlovich Laptev, Ning Dong, Norman Cheng, Oleg Chernoguz, Olivia Hart, Omkar Salpekar, Ozlem Kalinli, Parkin Kent, Parth Parekh, Paul Saab, Pavan Balaji, Pedro Rittner, Philip Bontrager, Pierre Roux, Piotr Dollar, Polina Zvyagina, Prashant Ratanchandani, Pritish Yuvraj, Qian Liang, Rachad Alao, Rachel Rodriguez, Rafi Ayub, Raghotham Murthy, Raghu Nayani, Rahul Mitra, Rangrabhu

Parthasarathy, Raymond Li, Rebekkah Hogan, Robin Battey, Rocky Wang, Russ Howes, Ruty Rinott, Sachin Mehta, Sachin Siby, Sai Jayesh Bondu, Samyak Datta, Sara Chugh, Sara Hunt, Sargun Dhillon, Sasha Sidorov, Satadru Pan, Saurabh Mahajan, Saurabh Verma, Seiji Yamamoto, Sharadh Ramaswamy, Shaun Lindsay, Shaun Lindsay, Sheng Feng, Shenghao Lin, Shengxin Cindy Zha, Shishir Patil, Shiva Shankar, Shuqiang Zhang, Shuqiang Zhang, Sinong Wang, Sneha Agarwal, Soji Sajuyigbe, Soumith Chintala, Stephanie Max, Stephen Chen, Steve Kehoe, Steve Satterfield, Sudarshan Govindaprasad, Sumit Gupta, Summer Deng, Sungmin Cho, Sunny Virk, Suraj Subramanian, Sy Choudhury, Sydney Goldman, Tal Remez, Tamar Glaser, Tamara Best, Thilo Koehler, Thomas Robinson, Tianhe Li, Tianjun Zhang, Tim Matthews, Timothy Chou, Tzook Shaked, Varun Vontimitta, Victoria Ajayi, Victoria Montanez, Vijai Mohan, Vinay Satish Kumar, Vishal Mangla, Vlad Ionescu, Vlad Poenaru, Vlad Tiberiu Mihailescu, Vladimir Ivanov, Wei Li, Wenchen Wang, Wenwen Jiang, Wes Bouaziz, Will Constable, Xiaocheng Tang, Xiaojian Wu, Xiaolan Wang, Xilun Wu, Xinbo Gao, Yaniv Kleinman, Yanjun Chen, Ye Hu, Ye Jia, Ye Qi, Yenda Li, Yilin Zhang, Ying Zhang, Yossi Adi, Youngjin Nam, Yu, Wang, Yu Zhao, Yuchen Hao, Yundi Qian, Yunlu Li, Yuzi He, Zach Rait, Zachary DeVito, Zef Rosnbrick, Zhaoduo Wen, Zhenyu Yang, Zhiwei Zhao, and Zhiyu Ma. The llama 3 herd of models, 2024.